# Solution-Induced Reconstructive Epitaxial Nucleation on Pseudoflat Surfaces of Fractal Gel-Grown Ammonium Chloride

**C. S. Strom***

*Serious Too Crystal Morphology Software, P.O. Box 2139, 1000 CC Amsterdam, The Netherlands*

**Xiang-Yang Liu**

*Department of Physics, The National University of Singapore, 10 Kent Ridge Crescent, Singapore 119260*

**Mu Wang**

*National Laboratory of Solid State Microstructures, Nanjing University, Nanjing 210093, China, and Center for Advanced Studies of Science and Technology of Microstructures, Nanjing 210093, China*

*Received: March 7, 2000; In Final Form: August 2, 2000*

The morphological manifestation of regular fractal patterns in ammonium chloride and the transition from ordinary to fractal morphology are studied at the crystallographic and molecular level by means of the Hartman−Perdok theory. The theoretically predicted growth forms as a function of growth conditions are in excellent agreement with experimental results for growth out of vapor ({211} and {110}) and out of polar solutions ({211}, {100}, and/or {111}), in the ordinary as well as fractal morphological regimes. The {211} surface is $(2 \times 1)$-reconstructed due to internal or structural energy gain that persists in all growth conditions. The mechanism responsible for the onset of fractal growth in a gel containing water and agarose molecules is solution-induced reconstructive epitaxial nucleation (SIREN) between pseudoflat pyramidal {211} faces. SIREN is equivalent to the structural match between crystallites, anticipated in the macroscopic theory of nucleation and growth kinetics [Liu, X. Y.; Strom, C. S.; *J. Chem. Phys.* **2000**, *113*. In press.]. It is associated with an increase in the effective surface supersaturation, brought about by the surface poisoning of the agarose inhibitors. It is characterized by a critical length parameter $\langle \bar{l} \rangle$ of the order of or lower than crystallite dimension, and a critical match parameter $m \rightarrow 1$, developed in that work.

## Introduction

Crystallites of ammonium chloride ($NH_4Cl$) exhibit two global morphological types. The ordinary regime contains naturally and synthetically grown crystallites exhibiting a variety of habits that depend strongly on the growth environment. Sometimes $NH_4Cl$ crystals undergo a trasformation from ordinary to fractal morphology depending on the growth medium. The fractal branching regime is obtained during growth from agarose gel and consists of faceted crystallites, with remarkable correlations in their crystallographic orientations. Previous theoretical treatments have not explained the growth forms of ammonium chloride in either the ordinary or fractal morphological regime or the transition from ordinary to fractal growth.

In an earlier investigation,[1] the theory of nucleation and growth kinetics was employed to describe, at the macroscopic level, the transition from the regular to the fractal morphology of ammonium chloride as caused by experimental conditions, notably surface supersaturation. That treatment focuses on the external effects without taking the internal structural aspects into account. The present theoretical treatment employs the Hartman−Perdok (HP) theory[2−5] to explain the regular morphology and the transition to the fractal regime as a function of growth conditions. This work introduces the microscopic mechanism by which that transition takes place in the form of surface reconstruction induced by the dual action of the polar water molecules and the agarose molecules of the gel. The results obtained here at the molecular and structural level are in satisfactory agreement with the macroscopic findings of ref 1, optical and AFM images of the fractal patterns,[6,7] and natural and synthetic specimens.[8]

After a brief review of the HP theory in section 2, the basic morphology of ammonium chloride is derived in two prevalent growth environments: vapor and aqueous solutions (sections 3 and 4). The theory is compared with experiment in the ordinary (section 5) and fractal (section 6) regimes. The molecular compositions of the theoretical growth layers reveal that a solution-induced reconstructive epitaxial nucleation (SIREN) mechanism brings about the transition from ordinary to fractal morphology, by joining the individual crystallites along {211} (section 7).

## 2. Summary of the Hartman−Perdok Theory

The Hartman−Perdok (HP) theory prescribes a method for determining the orientations and chemical compositions of all possible surface configurations that could function as growth layers. Surface compositions and orientations of flat (F) faces are determined as intersections of periodic bond chains,[2] and can be derived graph-theoretically.[4] A periodic bond chain (PBC) is a chain of strong bonds, or bonds in the first coordination sphere, between growth units. The strong bonds are the bonds formed when the growth units approach each other

* Corresponding author.

10.1021/jp000883g CCC: $19.00 © 2000 American Chemical Society
Published on Web 09/20/2000

during crystallization. A theoretical growth layer is called an F(flat)-slice and consists of two or more intersecting coplanar PBCs, with the face orientation defined by the PBC directions.

An F-slice must satisfy two basic requirements: first it must have stoichiometric composition, meaning that the basic block of the $NH_4Cl$ structure generating a growth layer (*hkl*) must contain one $NH_4$ cation and one Cl anion; second, the condition of "flatness" means that an F-slice must not contain lattice translations oblique to (*hkl*). If a network of stoichiometric composition, generated by means of combining PBCs, is considered with lattice translations oblique to the face, it is called a *pseudo-F-slice*.[3]

The ionic nature of ammonium chloride justifies the assumption that growth is predominantly an energy-driven process, in which entropic effects play a negligible role. Then, according to the Hartman−Perdok theory,[2,4,5,3] out of all theoretical F-slices, the actual growth layer configuration in each {*hkl*} orientation is triggered by the prevalent growth conditions in an energetically optimal way. The physical principle determining the orientations and chemical compositions of the growth layers is that the energy required to attach a new growth layer onto the existing structure in the presence of the mother phase, should be minimal.

*2.1. Internal or Structural Morphology in near-Vacuum Conditions.* The internal or structural morphology is the morphology for which the structure is responsible. It becomes manifest in growth out of near-vacuum conditions, i.e., vapor or a weakly interacting mother phase, low supersaturation, and insignificant kinetic effects, since then the external factors exercise minimal influence.

The energy quantities featuring in the energy balance equation $E_{cr} = E_{slice} + E_{att} + E_{dip}$ are described in detail in refs 2 and 3. The slice energy $E_{slice}$ is the energy per unit cell content per mole when a slice $d_{hkl}$ is formed.[2] The attachment energy is the amount of energy released per unit cell content per mole when the new layer $d_{hkl}$ attaches itself to the rest of the structure. The surface energy[2] $E_{surf}$ is the amount of work necessary to split a crystal isothermally and reversibly in two halves along (*hkl*) at infinite distance. And the specific energy $E_{spec}$ is the surface energy per unit area on (*hkl*). Finally, the dipole energy $E_{dip} \equiv -2\pi(d^{\perp})^2/V$ arises from the existence of a component of the dipole moment normal to the face. $V$ is the unit cell volume. $d^{\perp}$ is the component of the electric dipole moment of the unit cell generating the F-slice, perpendicular to the (*hkl*) face. $E_{suppl} \equiv E_{cr} - E_{slice}$ is the supplement of the slice energy. For apolar faces $d_{\perp} = 0$, hence $E_{suppl} = E_{att}$. The total crystal energy $E_{cr}$ is a constant, all other energies depend on the orientation of the surface. The electrostatic energy quantities are calculated exactly and free from adjustable parameters by employing a two-dimensional Ewald summation.[5] In the broken bond model the energies amount to numbers counting the occurrence of the various bond types in the structure.

The growth form that results when the external effects are either negligible or in a first approximation neglected, is called the "internal" or "structural" morphology.[2] Because vapor is the closest appoximation to a theoretical vacuum, the morphology resulting when growth occurs from sublimation is the closest approximation to the internal morphology. Then the most important F-slices are the geometrically compact and hence energetically optimal. The actual growth layer in a face {*hkl*} is the one that has a maximum magnitude of the slice energy or a minimum magnitude of the attachment energy.[2,5,3] For a given {*hkl*} the minimum magnitude of the attachment energy or of the supplementary-slice energy is taken proportional to the growth rate.

In ionic compounds such as ammonium chloride, polarity is an essential element in controlling growth. The surface polarity is intimately related to the polarity properties of the growth medium. In near-vacuum conditions polar surfaces are unstable because the electrostatic potential does not converge on surfaces with a net normal dipole moment.[3] Consequently dipoleless faces, that usually have large slice energy magnitudes, dominate the growth habit. In the absence of dipoleless surface configurations, in near-vacuum conditions, polar surfaces tend to stabilize themselves by internal or structural effects, depending on the properties of the individual molecules, e.g., flexibility, and the configurational pattern at the surface in question. Various mechanisms tend to decrease surface energy by redistribution of charges at the surface; adjustment of bonds at the surface; and surface relaxation or surface reconstruction leading to a dipoleless F-slice.

*2.2 External Factors Affecting the Morphology in Strongly Interacting Polar Medium.* The actually observed morphology is the composite result of the internally determined morphology and external effects such as growth kinetics and interaction between the growth front and the mother phase. In growth out of a strongly interacting medium the actual growth fronts are those for which the surface−liquid interaction is maximum. It is experimentally observed that growth out of a nonpolar medium tends to enhance the prominence of faces parallel to nonpolar F slices, whereas growth out of a polar medium tends to enhance the prominence of faces parallel to polar F-slices. The energetically optimal surfaces in the presence of a polar solution are the polar rather than the dipoleless surfaces, because they react most strongly with polar solution particles such as water molecules. The dipole moments of the polar particles interact with the surface dipole by aligning themselves with the site electric field.[9] The tendency to maximize the interaction between the growth front and the adjacent liquid can be seen as an external mechanism for stabilizing polar surfaces.

Another external effect controlling the morphology is surface poisoning (the interaction between the growth front and impurities or inhibitor particles present in the solution). It causes a decrease in the growth rate of that face and consequently an increase in its morphological significance.

## 3. Application by the Hartman-Perdok Theory to Ammonium Chloride

*3.1. Derivation of Growth Layers.* The $NH_4Cl$ structure crystallizes in space groups $Fm\bar{3}m$ and $Pm\bar{3}m$. The structure has been determined by various groups in the space group $Pm\bar{3}m$ with one formula unit $Z = 1$ in the asymmetric portion of the unit cell.[10−13] The *a*-axis in Å is reported equal to 3.860[10,11] and 3.8771(2);[13] a modification is reported[12] with $a = 6.533$ Å.

The N and Cl atoms are located at (0, 0, 0) and ($^1/_2$, $^1/_2$, $^1/_2$), respectively. In refs 10, 12, and 13 the four H atoms, belonging to the $NH_4$ molecule, and surrounding N in tetrahedral coordination, could not be located in the unit cell. However, ref 11 gives positions of H at (0.146, 0.146, 0.146), in which case the multiplicity of the space group generates eight hydrogen positions corresponding to each ammonium. Therefore, in employing the results of ref 11, the distribution of the four hydrogen atoms surrounding each ammonium must be taken as the eight symmetry-generated sites occupied statistically. In all works,[10−13] the nominal atomic charges are reported as

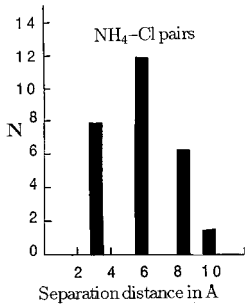


**Figure 1.** Histogram of number of $NH_4-Cl$ pairs $N$ versus separation distance. The first minimum at $-d = 3.52$ Å marks the radius of the first coordination sphere. (Second and third coordination spheres are just beyond −6.00 and −8.5 Å, respectively.)

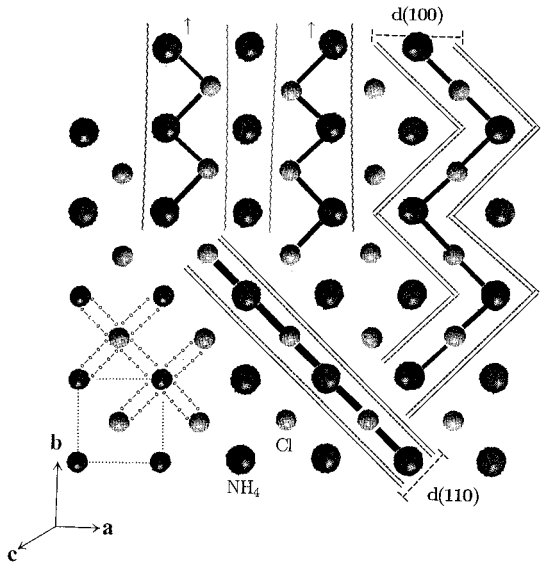


**Figure 2.** Structure projection on (001) showing the first coordination spheres of Cl (small gray spheres) and $NH_4$ (large black spheres). The dashed−dotted lines mean strong bonds. Different bonds are shown coinciding in projection. There is a single $d_{110}$ F-slice, and a pair of polar $d_{100}$ F-slices. The strong bonds within the F-slices are indicated by bold thick solid lines. The $NH_4^+$- and $Cl^-$-boundaries of the pair are marked by bold and thin wavy lines, respectively. The boundaries of the dipoleless $d_{110}$ and a hypothetical reconstructed $2d_{100}$ are marked by double lines.

$q_{Cl} = -1$, $q_N = -3$, and $q_H = +1$. When the four hydrogens of each ammonium are taken statistically distributed over eight positions, the hydrogen charge must be taken as half the nominal value, $q_H = +\,^1/_2$. In this work we use $a = 3.8756$ Å,[14] and consider the H atoms distributed statistically over the eight symmetrically equivalent positions (0.146, 0.146, 0.146). The nominal charge on N is −3 and on each of the eight H atoms is + 0.5, the charge on Cl is −1.

The growth units in ammonium chloride are the $NH_4$ cations, with mass centers at the locations of N, and Cl anions. The strong bonds are obtained from the histogram of Figure 1, depicting the number of $NH_4^+-Cl^-$ pairs versus separation distance. At a distance of 3.5152 Å, which is the radius of the first coordination sphere, the number of cation−anion pairs reaches a minimum of zero; within ≤3.5152 Å there are eight strong bonds. Figures 2 and 4 show the strong bonds of $NH_4Cl$ projected on (001) and (01$\bar{1}$), respectively. Program FFACE[4] derives the orientations and compositions of all possible growth layers, called F-slices, graph-theoretically in terms of networks. PBCs exist in directions ⟨100⟩, ⟨110⟩, and ⟨111⟩. Forms {100}, {110}, {111}, and {211} contain intersecting PBCs. The first

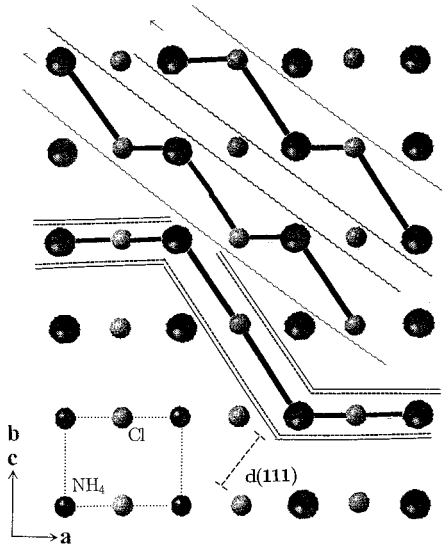


**Figure 3.** Structure projection on (01$\bar{1}$) showing the pair of polar F-slices $d_{111}$, together with a hypothetical dipoleless reconstructed $2d_{111}$ layer. The first coordination spheres of $NH_4$ and Cl in this projection are shown in Figure 4. The bonds within each F-slice and the slice boundaries are marked as in Figure 2.

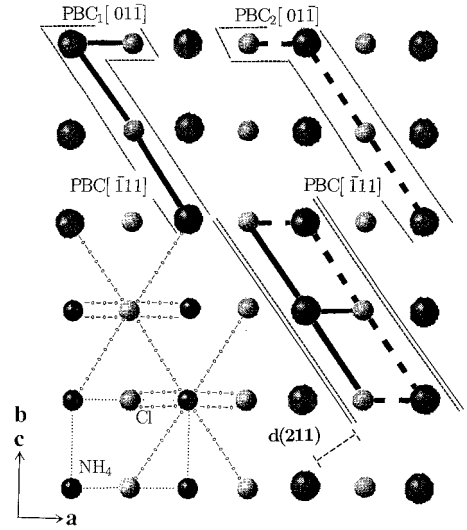


**Figure 4.** Structure projection on (01$\bar{1}$) showing layers in {211}. First coordination spheres of $NH_4$ (large black spheres) and Cl (small gray spheres). Dashed−dotted lines are strong bonds, double such lines imply two different strong bonds coinciding in projection. The bonds within each of the pair of pseudo-F-slices in (211) are distinguished by bold thick solid and dashed lines, respectively. Their boundaries are shown by single dashed lines. The proposed reconstructed F-slice $2d_{111}$, formed by a combination of the two, is bounded by double-dashed lines. Epitaxial nucleation is assumed to operate via the $2d_{111}$ layer. The borderline between crystallites A and B in Figures 6a abd 7b is indicated by the transition from bold thick solid to dashed lines representing the bonds belonging to A and B, respectively.

three faces are F(flat) since they contain F-slices. {211} contains no valid F-slices but only a single pseudo-F-slice.

Figure 2 shows the hexahedral {100} F-slices and the dodecahedral {110} F-slices in a structure projection on (001). Figure 3 shows the octahedral {111} F-slices in a structure projection on (01$\bar{1}$). We see that the opposite boundaries of the single F-slice $d_{110}$, marked by double lines in the figure, are related by a symmetry point located in the middle of the layer. That symmetry forces the surface dipole of $d_{110}$ to vanish. In {100} and {111} the F-slices come in pairs. The opposite boundaries corresponding to distinct F-slices belonging to a pair

**TABLE 1: Slice $E_{Slice}$ and Attachment $E_{Att}$ Energies in the Broken Bond Model[a]**

| flat face (*hkl*) | bonds $NH_4 \rightarrow Cl$ | bonds $Cl \rightarrow NH_4$ | total in unit cell |
|---|---|---|---|
| $E_{slice}(110)$ | 4 | 4 | 8 |
| $E_{slice}(100)$ | 4 | 4 | 8 |
| $E_{slice}(111)$ | 3 | 3 | 6 |
| $E_{att}(110)$ | | | |
| top boundary | 2 | 2 | 4 |
| bottom ≡ top | 2 | 2 | 4 |
| total over boundaries | 4 | 4 | 8 |
| $E_{att}(100)$ | | | |
| $NH_4^+$ -boundary | 4 | 0 | 4 |
| $Cl^-$-boundary | 0 | 4 | 4 |
| total over boundaries | 4 | 4 | 8 |
| $E_{att}(111)$ | | | |
| $NH_4^+$-boundary | 4 | 1 | 5 |
| $Cl^-$-boundary | 1 | 4 | 5 |
| total over boundaries | 5 | 5 | 10 |

[a] Number of bonds per $NH_4$ molecule ($NH_4 \rightarrow Cl$), and number of bonds per Cl molecule ($Cl \rightarrow NH_4$); the sum is the number of bonds per unit cell. Attachment energies are specified explicitly in terms of the bonds crossing the individual slice boundaries (as labeled in the figures). The total attachment energies are the sums over opposite lying boundaries. The crystal energy is 16 bonds per unit cell content.

are related by symmetry, but opposite boundaries of one and the same F-slice are symmetrically distinct. The $NH_4^+$-boundaries of $d_{100}$ and $d_{111}$ are marked by bold wavy lines; the $Cl^-$-boundaries are marked by thin wavy lines. The pair of $d_{100}$ F-slices have equal and opposite surface dipoles $\pm 1.9378\ e$Å. The pair of $d_{111}$ F-slices have equal and opposite surface dipoles $\pm 1.1188\ e$Å.

In Figure 4 it is easy to see in a structure projection on $(01\bar{1})$ why the would-be networks in face {211} could never define valid growth layers. There are three PBCs parallel to {211}: one chain in direction $[\bar{1}11]$

$$PBC[\bar{1}11] \equiv NH_4[000] \rightarrow Cl[\bar{1}00] \rightarrow NH_4[111]$$

and two chains in direction $[01\bar{1}]$

$$PBC_1[01\bar{1}] \equiv NH_4[000] \rightarrow Cl[00\bar{1}] \rightarrow NH_4[01\bar{1}]$$

$$PBC_2[01\bar{1}] \equiv NH_4[000] \rightarrow Cl[\bar{1}0\bar{1}] \rightarrow NH_4[01\bar{1}]$$

The combination $PBC[\bar{1}11] \times PBC_1[01\bar{1}]$ involves a lattice translation $[10\bar{1}]$ between indispensable Cl anions. Similarly, the combination $PBC[\bar{1}11] \times PBC_2[01\bar{1}]$ involves a lattice translation [1 0 0] between indispensable Cl anions. Removal of any of the indispensable Cl ions leaves the network disconnected. While on the other hand maintaining the out-of-face-translations results in loss of the "flatness" characteristic. In ammonium chloride {211} is unique in being the only pseudo-F form.

*3.2. Energy Quantities.* The broken bond model has a transparent simplicity but cannot provide a reliable assessment of the energy quanities for ionic compounds. It is presented because it provides insight in the surface structure. The energy quantities are numbers counting the occurrence of the only bond type in the structure, $NH_4^+-Cl^-$. The total crystal energy per unit cell content equals the coordination of $NH_4^+$ (8 $NH_4^+ \rightarrow Cl^-$ bonds) plus the coordination of $Cl^-$ (8 $Cl^- \rightarrow NH_4^+$ bonds) = 16 bonds. Table 1 shows the broken bond slice and attachment energies of the F-slices per molecule and per unit cell. The attachment energies are further broken down in terms of the bonds crossing each boundary.

**TABLE 2: Coulomb Energies of the F-Slices of Ammonium Chloride in the Statistical Point-Charge Model in Which N Is Surrounded by Eight Statistically Distributed H Atoms[a]**

| F face | $E_{slice}$ | $E_{att}$ | $E_{dip}$ | $E_{suppl}$ | $E_{spec}$ |
|---|---|---|---|---|---|
| (110) | −7.6785 | −0.08162 | 0 | −0.08162 | −0.3690 |
| (100) | −7.3835 | +0.02869 | −0.4053 | −0.3766 | −0.4877 |
| (111) | −7.6204 | −0.00464 | −0.1351 | −0.1397 | −0.2939 |

[a] Point charges taken as $q_N = -3$, $q_H = +0.5$, $q_{Cl} = -1$. Slice $E_{slice}$, attachment $E_{att}$, dipole $E_{dip}$, and supplementary-slice $E_{suppl} \equiv E_{cr} - E_{slice}$, energies are given in $e^2$/Å, where $e$ is the elementary charge. Specific surface $E_{spec}$ energies in $e^2$/Å$^3$. The constant crystal energy is $E_{cr} = -7.7601\ e^2$/Å.

Table 2 is an analogous list of electrostatic energy quantities calculated exactly and free from adjustable parameters by employing a two-dimensional Ewald summation.[5] They depend only on the previously adopted formal point-charge asignments. The van der Waals contributions are left out of consideration because they are relatively negligible. The relevant energy quantities here will be the slice, dipole and supplementary-slice energies. The attachment energies and remaining energy quantities[5] are presented for completeness.

Table 2 with Figures 2 and 3 shows that $d_{100}$ and $d_{111}$ have similar electrostatic surface structure, whereas Table 1 shows that they have dissimilar surface bonding patterns.

Because of the simplicity of the ammonium chloride structure, the surface behavior can be deduced by inspecting the results tabulated in Table 2.

The dodecahedron $d_{110}$ (Figure 2) is the only F-slice in {110}, and the only dipoless growth layer possible in the entire structure. It is geometrically compact and hence energetically optimal, as can be seen from the large magnitude of its slice energy ($-7.6785\ e^2$/Å in Table 2). The low magnitude of the attachment energy ($-0.08162\ e^2$/Å in Table 2) results in a low growth rate for {110}, and consequently a high morphological importance for {110}.

All hexahedral and octahedral surfaces are strongly polar and hence unstable in vacuo (subsection 2.1). The dipole energy of $d_{100}$ ($-0.4053\ e^2$/Å in Table 2) is high, even to the extent of causing a positive amount of attachment energy, indicating repulsion between that layer and the underlying structure.

## 4. Surface Behavior and Theoretical Morphology

Two of the three internal stabilization mechanisms for the polar surfaces {100} and {111}, i.e., redistribution of charges and adjustment of bonds at the surface, are unlikely to be effective in a substantial way, given the relatively strong ionic nature of the $NH_4-Cl$ bonds. The third possible internal stabilization mechanism, a $2 \times 1$ surface reconstruction, could only lead to surface stabilization by neutralizing the surface dipole, if it was energetically favorable. The right-hand portion of Figure 2 shows a possible $2d_{100}$ reconstructed dipoleless growth layer, obtained as a combination of the two polar $d_{100}$ F-slices. The lower portion of Figure 3 shows a possible $2d_{111}$ reconstructed dipoleless growth layer, obtained as a combination of the two polar $d_{111}$ F-slices. The boundaries of these hypothetical reconstructed layers are marked by double lines. The strongly undulated character of $2d_{100}$ and $2d_{111}$ indicates that such reconstruction would hardly bring about any energy gain and hence is unlikely to occur.

A possible external stabilization mechanism, tending to maximize the crystal−fluid interaction, could take effect if the {100} and {111} polar surfaces were brought in contact with polar solution particles such as water molecules. The opposite boundaries of the $d_{100}$ and $d_{111}$ F-slices are terminated by $NH_4^+$

molecules on one side, and $Cl^-$ ions on the other. We have already established that the $NH_4^+$-boundaries of $d_{100}$ and $d_{111}$ have similar electrostatic surface structures, and that also holds true for the $Cl^-$-boundaries (see Figures 2 and 3).

Which of the two alternatively possible surface terminations adjacent to the near-surface liquid will actually materialize, depends on whether the $NH_4^+$- or the $Cl^-$-terminated surfaces interact more strongly with the solution. In aqueous solutions the water molecules and impurities possessing charge distributions will certainly distinguish between $NH_4^+$ versus $Cl^-$ surface terminations, but they can hardly distinguish between $d_{100}$ versus $d_{111}$ growth layers. This similarity between $d_{100}$ and $d_{111}$ in any event tells us that the growth fronts of both {100} and {111} will consist of $NH_4^+$, *or* that both will consist of $Cl^-$, and that the solution will interact in a similar way with either the {100} or the {111} adjacent surface.

Under which conditions {100} or {111} will prevail depends on the detailed properties of the solution particles. Some particles could moreover discriminate between the $NH_4^+$-boundary of $d_{100}$ versus that of $d_{111}$, or the $Cl^-$-boundary of $d_{100}$ versus that of $d_{111}$. If such additional influence is weak or absent, then {100} and {111} would have comparable morphological significance; otherwise, one of the polar forms will supress the other.

The boundaries of the pseudo-F $d_{211}$ layers are marked in Figure 4 by single dashed lines. The out-of-face lattice translations of the $Cl^-$ ion induce large equal and opposite dipole moments normal to that surface. Each $d_{211}$ layer is strongly polar and unstable. Obviously if a $2 \times 1$ reconstruction were to occur on the icosahedral pseudo-F form {211}, a highly stable, dipoleless, planar and compact $2d_{211}$ growth layer would result, with an enormous energy gain in that face. The boundaries of $2d_{211}$ are marked by double lines in Figure 4. Energy quantities for the pair of {211} pseudo-F-slices and the reconstructed F-slice $2d_{211}$ are not included in Table 2, where only genuine and unreconstructed F-slices are tabulated. Figure 4 shows that the slice energy of $2d_{211}$ per molecule would be enormous. The theoretical basis for a {211} surface reconstruction is so compelling, that such reconstruction is anticipated under most circumstances, regardless of the nature of the growth environment. Then {211} should appear pronounced in *both* near-vacuum and polar environments *even though* it is theoretically not an F(flat)-form!

*In conclusion*, first, since reconstruction of the polar and unstable {100} and {111} in vacuo is energetically unlikely, in growth out of near-vacuum conditions these polar forms would be totally suppressed by the dipoleless F-slice $d_{110}$ in combination with $2d_{211}$. Second, polar solution particles serve as a stabilizing mechanism by interacting with the polar {100} and {111} surfaces, thus enabling $d_{100}$ and $d_{111}$ to attain low enough growth rates to become morphologically significant. That interaction takes place mostly through *either* the $NH_4^+$-boundaries *or* the $Cl^-$-boundaries of *both* growth layers $d_{100}$ *and* $d_{111}$. In general $d_{100}$ and $d_{111}$ should feature on the same habit, in combination with $2d_{211}$. Depending on the specific details of the solution, $d_{100}$ may prevail at the cost of $d_{111}$ or vice versa, but in any case in combination with $2d_{211}$. (See Figures 2−4.)

### 5. Comparison between Theory and Experiment in Ordinary Morphology

The ordinary morphological regime corresponds to growth conditions of low surface supersaturations.[1]

Ammonium chloride occurs naturally as the mineral sal-ammoniac and is the most common ammonium-bearing mineral.

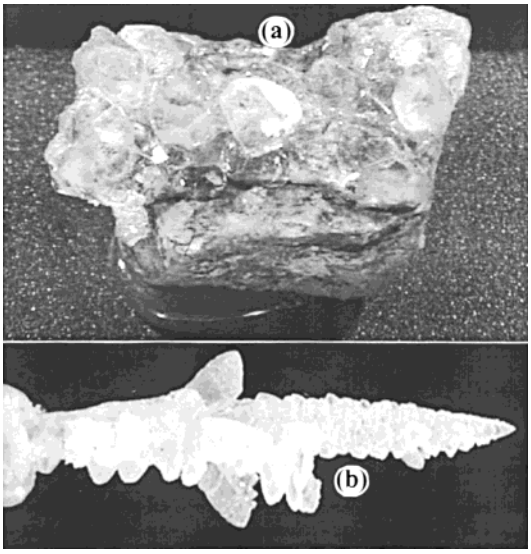


**Figure 5.** (a) Natural specimens, and (b) natural dendritic growth of sal-ammoniac.[15]

It is an unusual halide owing its peculiar properties to the content of ammonium. Sal-ammoniac crystallizes by sublimation, out of gases escaping from volcanic rocks.[15] Often no liquid phase is involved in the formation of the mineral. The small, delicate and short-lived crystals are very soluble in water. The mineral habit includes cubes, octahedra, and dodecahedra, (Figure 5a). Also complicated arborescent, snowflake-like, and dendritic specimens are found (Figure 5b).

The Groth Atlas[8] gives the following account of the faces encountered on $NH_4Cl$ samples grown naturally out of vapor or aqueous solutions. The form {211} is the most prominent form in both cases of growth by sublimation and from aqueous solutions. The main form encountered in crystals grown by sublimation is {110}. Growth from aqueous solutions results predominantly in {111} and/or {100}. {100} becomes more pronounced when ionic compounds such as $CaCl_2$ and $CdCl_2$ are added to the aqueous solution. A variety of spurious forms such as {311}, {310}, {411}, and {522} are encountered occasionally. The theoretical predictions of the previous section are in excellent agreement with the experimental results.

Recently attempts have been undertaken to study the morphology of compounds isomorphous to ammonium chloride, in particular cesium halides,[16] by processing the so-called interference effect among multiple networks of bonds between molecular mass centers. These networks satisfy some of the properties of the theoretical F-slices, and result from the definitions and methods of ref 4. This approach based on "interference effects" follows from the original theoretical treatment of ref 17. The bonding patterns of these isomorphous structures are the same, hence so are the networks. If knowledge of the networks sufficed to predict the final morphology, then the growth forms of these halides should, under identical growth conditions, be identical with the observed forms of ammonium chloride. The observed large discrepancies under *all* experimental conditions between various halides indicate that the atomic information on the growing crystal surfaces plays a key role in the morphology, but becomes irrevocably lost in restricting the analysis to bonds between molecular mass centers.

### 6 Comparison between Theory and Gel Experiments

The gel contains agarose molecules in aqueous solution. According to the discussion in section 4, forms {100}, {111},

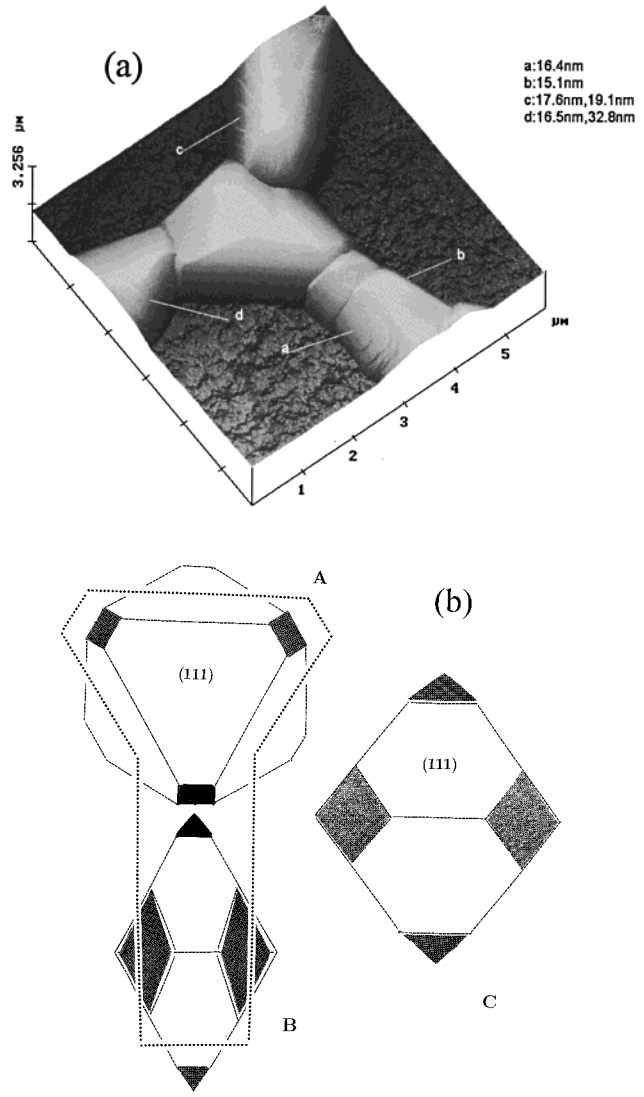


**Figure 6.** (a) AFM image of experimental growth forms of ammonium chloride, where {111} dominates and {100} is inhibited by SIREN. (c) Crystallites A and C are undeformed and projected on planes ⊥ [111] and ⊥ [110], respectively. Crystallite B is C after elongation. The crystallites are indexed according to scenarios (1a−c) of Table 3. The major form is {111}. Gray faces are secondary forms or side faces. Black faces are nucleation areas. Gray and black faces can be indexed alternatively as {100} or as the tetragonal-pyramidal {211} faces. Best agreement is obtained with the indexation {211} for the nucleation region, scheme (1b) or (1c) in Table 3. Preferred growth direction: ⟨100⟩. Dotted lines isolate the regions of crystallization visible in the photographs.

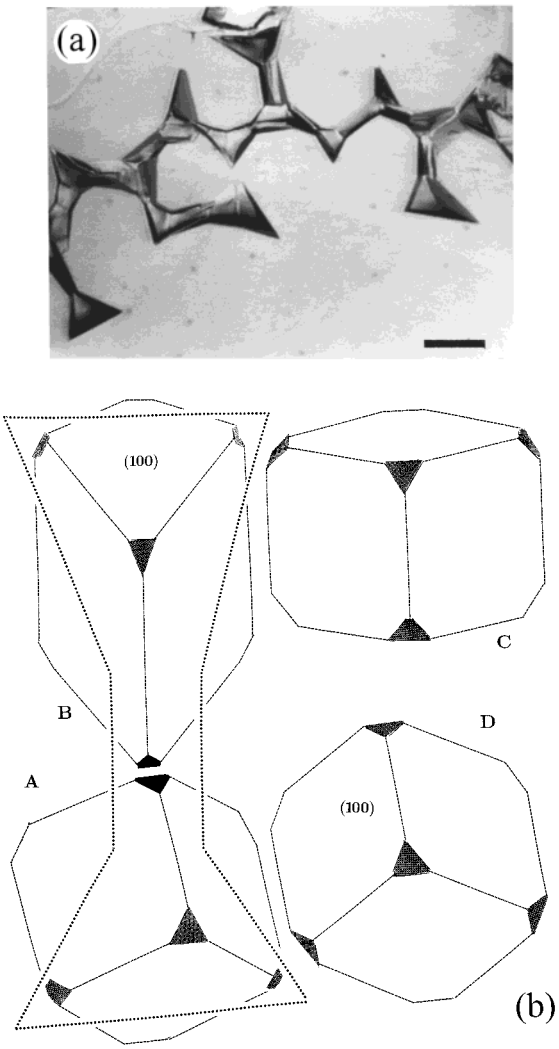


**Figure 7.** (a) Fractal growth pattern of ammonium chloride, where {100} dominates and {111} is inhibited by SIREN. (b) Crystallites A, C and D are undeformed and projected on planes ⊥ [211], ⊥ [331], and ⊥ [111], respectively. Crystallite B is C after elongation. The crystallites are indexed according to scenarios (2a,b) of Table 3. The major form is {100}. Gray faces are secondary barely discernible {111} forms. The black faces are nucleation areas and can be indexed alternatively as {111} or as the trigonal-pyramidal {211} faces. Best agreement is obtained with the indexation {211} for the nucleation region, scheme (2b) in Table 3. Preferred growth direction: ⟨111⟩. Dotted lines isolate the regions of crystallization visible in the photographs.

and {211} are expected to feature in the fractal morphology. The water and agarose molecules will interact with either the $NH_4^+$-boundaries or the $Cl^-$-boundaries of $d_{100}$ and $d_{111}$. The hexahedral {100} and octahedral {111} surfaces should have comparable morphological importance and probabilities of occurrence; they would be expected to appear in the same habit at least some of the time. However, they are never observed together on the same fractal pattern. Furthermore, no {211} form is visible in fractal growth.

Owing to lack of accuracy and reliability of the data as far as detailed experimental features are concerned (see, e.g., delineation of angles and registered step heights in Figure 6a), we are compelled to restrict attention to the global morphological features of the experimental outcome. The dodecahedron, either by itself or in combination with any other candidate F-forms, is definitely absent from the images of Figures 6a and 7a. The experimental growth forms also preclude the combinations {110}−{100} and {110}−{111}. The visual impression of the octahedron {111} as dominant form gives the best match with the AFM image in Figure 6a. The visual impression of the hexahedron {100} as dominant growth form gives the best match with the optical image in Figure 7a. The above impressions are especially true when allowance is made for alternating periodic elongation of some crystals during growth, together with the absence of the lower portions of the crystals due to mechanical constraints.

The theoretical discussion of section 4 gave a satisfactory explanation as to why the dipoleless, most compact, and in vacuo energetically optimal dodecahedral form {110} does not occur. The absence of {110} simply confirms the known properties of the gel, i.e., that it contains water molecules. Because of their similar electrostatic surface structures, the polar faces {100} and {111} may be expected to be of comparable

**TABLE 3: Indexation Scenarios (1a,b,c) of Figure 6A, and (2a,b) of Figure 7A[a]**

| scenario | primary form | nucleation region | secondary or side form | agreement with theory | agreement with image | symmetry properties | growth direction |
|---|---|---|---|---|---|---|---|
| (1a) | {111} | {100} | {100} | slight | slight | preserved | ⟨100⟩ |
| (1b) | {111} | {211} face | {211} pyramid | good | some | preserved | ⟨100⟩ |
| (1c) | {111} | {211} face | {100} | good | good | hypomorphic B | ⟨100⟩ |
| (2a) | {100} | {111} | {111} | slight | good | preserved | ⟨111⟩ |
| (2b) | {100} | {211} face | {111} | good | good | preserved | ⟨111⟩ |

[a] Crystallite type A is undistorted, type B is elongated in the preferred direction of growth. Primary forms are {111} (Figure 6) and {100} (Figure 7). Nucleation regions are black and secondary or side faces are gray in these figures.

morphological importance, unless some additional mechanism operated to obscure one of these faces in the presence of the other. This is confirmed by the present experimental results. Figures 6 and 7 show two different habit types, to the extent to which these are discernible, given the poorly controlled experimental conditions.

The observed nucleation shows uninterrupted periodicity and consistency with respect to crystallographic orientation. The crystallographic orientations of the $NH_4Cl$ crystallites were analyzed after classifying them in types A and B, shown in Figures 6b and 7b. The experimental results show that the A and B crystallites alternate strictly in Figure 6a, and more loosely in Figure 7a. The task ahead is first, to index the primary and secondary faces in the AFM image of Figure 6a and the optical image of Figure 7a; second, to determine the faces along which nucleation occurs; and third, to explain the nucleation mechanism.

Having adopted the indices {111} for the primary faces in the AFM image (Figure 6a), there remain two plausible indexations for the secondary faces which are: the small faces of crystallites A and B along which nucleation occurs, and the side faces of the elongated crystallite B. The possible indices are the F-form {100} or the tetragonal-pyramidal pseudo-F-faces {211}, according to scenarios (1a−c) of Table 3. The assignment of the side face as {100} in the AFM image agrees with a detail in the image of Figure 6a, showing clearly a cubic shape on a visible step on a side face. However that step shape may be distorted as a result of the elongation of the type B crystallite. The angular relations between the various crystallites in Figure 6a do not agree with the assignment {100} to the nucleation planes. The geometrical details show that pairs of {211} faces function as nucleation planes after undergoing a rotation $[01\bar{1}] \leftrightarrow [\bar{1}02]$.

In the optical image (Figure 7a) the primary and side faces are {100}, so that the possible indices for the nucleation face are the F-form {111} or the trigonal-pyramidal pseudo-F-faces {211}, according to scenarios (2a,b). By comparing Figure 7a,b we notice that the relative orientations assumed by crystallites A and B are fairly well reproduced when the normal to the projection plane for crystallite A is taken in direction [211]. This means that nucleation occurs by joining the face (211) of crystallite A with face $(\bar{2}\bar{1}\bar{1})$ of crytallite B. If the nucleation occurred along the {111} faces, crystallite A would appear in the same orientation as crystallite D shown projected normal to [111] in Figure 7b.

The preferred direction of growth in Figure 6 is ⟨100⟩, regardless of whether the {100} faces or the tetragonal-pyramidal {211} faces function as nucleation planes. Similarly, the preferred direction of growth in Figure 7 is ⟨111⟩ regardless of whether the faces {111} or the trigonal-pyramidal {211} faces function as nucleation planes.

The scenarios of Table 3 carry their specific merits and drawbacks listed in columns 5−7. The most plausible scenarios in Table 3 are (1b) or (1c)—the difference in experimental outcome between these two concerns a detail—and (2b). The geometrical details of pattern formation favor the pyramidal {211} assignment to the nucleation planes of the crystallites. This experimental result is consistent with the theoretical observation that the assignments {100} and {111} as nucleation regions in Figures 6a and Figure 7a, respectively, are unlikely. The reason is that these assignments leave unanswered two questions: first, the theoretical question why the chemically and electrostatically similar surfaces {100} and {111} should exhibit such diverse behavior; second, the observational question why the {211} form, so dominant in natural occurrences of this compound, should be totally absent in gel-growth experiments.

*In conclusion*, first, in the crystallites of Figure 6 the morphology is dominated by {111} while {100} is masked by the epitaxial nucleation mechanism. Second, in the crystallites of Figure 7 the morphology is dominated by {100} while the epitaxial nucleation operates to mask {111}. Third, in *both cases* that epitaxial nucleation mechanism operates on the unique pseudo-F {211} faces by surface reconstruction.

### 7. Solution-Induced Reconstructive Epitaxial Nucleation (SIREN)

We introduce an explanation at the crystallographic and molecular levels for the onset of the observed regular fractal branching, through solution-induced reconstructive epitaxial nucleation (SIREN) on the pseudo-F surfaces. Subsequently we show its equivalence with the macroscopic formulation of nucleation and growth kinetics of ref 1.

From the crystallographic point of view, the surface reconstruction along the faces of the {211} pyramid serves as agent for epitaxial nucleation. The highly polar $d_{211}$ pseudo-F-slices belonging to the respective crystallites, indicated by bold thick solid and dashed bonds in Figure 4, form a pair and combine so as to produce a nonpolar, highly stable and energetically optimal $2d_{211}$ growth layer. Because the crystallites are joined through the {211} pyramidal faces, the {211} form is never visible in any of the fractal patterns. In contrast, the absence of the epitaxial agent in the ordinary morphological regime allows the icosahedral form {211} to be prominently visible.

In the octahedral modification of Figure 6, epitaxial nucleation joins a pair of tetragonal pyramidal pseudo-flat {211} surfaces by aligning $[01\bar{1}] \leftrightarrow [\bar{1}02]$, and consequently it blocks the hexahedral form. In the hexahedral modification of Figure 7, epitaxial nucleation joins a pair of trigonal pyramidal pseudo-flat {211} surfaces by $(211) \leftrightarrow (\bar{2}\bar{1}\bar{1})$, and consequently it blocks the octahedral form. For this reason either the octahedral or the hexahedral form is observed in fractal growth, while both forms together are never observed on the same fractal pattern. In contrast, the absence of the epitaxial agent in the ordinary morphological regime allows for the simultaneous occurrence of both hexahedral and octahedral forms on the same crystal.[8]

Finally, the geometrical features of the images in Figures 6a and 7a show that the epitaxial mechanism amounts to nothing

other than the "structural match" between the substrate surface and the nucleating crystal surface, foreseen at the macroscopic level by the theory of nucleation and growth kinetics developed in ref 1. Here, at the microscopic level, that structural match takes effect through the $2 \times 1$ reconstruction on {211}. Figure 4 amounts to the crystallographic and molecular counterpart of Figure 1b in ref 1.

The final task is to explain why the presence of the gel should be critical to the transition from the ordinary to the fractal morphological regimes. These regimes are characterized by the aforementioned structural match parameter $m$ and the elemental branching period $\langle\bar{l}\rangle$.[1] In the ordinary regime, $\langle\bar{l}\rangle$ far exceeds the crystallite dimension. Regular fractal branching patterns set in as $\langle\bar{l}\rangle$ approaches values of the order of or lower than the crystallite dimension. Random fractal patterns are anticipated upon a further decrease of $\langle\bar{l}\rangle$, see Figure 4 of ref 1.

The regular fractal branching regime observed here is marked by the structural match at $m \rightarrow 1$, a value of $\langle\bar{l}\rangle \sim$ crystallite dimension, and an increase in the surface supersaturation. The action of the agarose molecules in the gel accounts for the increased surface supersaturation. These molecules are elongated, relatively rigid and have many hydrophilic interaction points. The nature of their strong interaction with the surfaces of ammonium chloride is physical and entropic. The agarose molecules act as blockers at locations accessible to the structure particles.[1] The surface poisoning due to the agarose inhibitor causes an increase in the effective surface supersaturation that is necessary for the transition to the fractal regime.[1]

## 8. Open Questions

The first major question that arises is why the structural matching prescriptions of the octahedral and hexahedral modifications should be different. In other words, why does the epitaxial mechanism in the hexahedral modification occur via $(211) \leftrightarrow (\bar{2}\bar{1}\bar{1})$ whereas in the octahedral modification it takes place via $[01\bar{1}] \leftrightarrow [\bar{1}02]$? In the absence of detailed energy calculations, the cause of this rotation remains unexplained. Undertaking the task of calculating the interaction energy between rotated {211} surfaces is only meaningful when improved experimental results become available, and it is out of the present scope.

The second major question is why the {211} form, which functions as a means of bringing about self-epitaxial nucleation, should, within the limits of observation, be absent from the remaining parts of the crystals? The high multiplicity of the form {211} implies that some {211} faces should still be visible elsewhere in the crystal. The absence of a subfamiliy of symmetrically related high-index {*hkl*} faces is known as hypomorphism. This effect has been persistently observed experimentally for high multiplicity faces, e.g., in experiments on ammonium dihydrogen phosphate,[18] which is a compound that also grows out of aqueous solutions. Since hypomorphism has thus far defied all attempts at theoretical explanation, it is impossible to either prove or disprove its existence in the case under study.

The optical image of Figure 7a gives the impression that the elemental branching period[1] $\langle\bar{l}\rangle \sim$ crystallite dimension is less strictly observed than in Figure 6a. The question arises whether this might be related to the distinction between hexahedral and octahedral modifications. Pivotal to the increase of the effective surface supersaturation in the fractal regime is the blocking action of the agarose molecules on the polar surfaces. The third major question therefore concerns the specific dual role played by the agarose inhibitors, as well as the experimental conditions in which the octahedral or hexahedral modification should dominate. Furthermore, energy calculations beyond the present scope are needed to determine whether the $NH_4^+$ or $Cl^-$ surface terminations of the polar faces interact more stronly with the polar water molecules and the large rigid agarose molecules.

A final minor question is whether the cause of the elongation of the crystallites should be sought in the mechanical strain imposed by the shape of the gel.

## 9. Conclusions

The Hartman-Perdok theory predicts for ammonium chloride a habit dominated by the dodecahedron {110} in growth out of near-vacuum, and by the hexahedron {100} and/or octahedron {111} in growth out of polar solutions. The {211} icosahedral form is predicted to feature just as prominently regardless of the growth medium, because the large energy gain attained through $2 \times 1$ surface reconstruction persists under most conditions. Indeed, the basic growth forms of synthetic and natural crystals grown by sublimation include {110} and {211}; those grown from various impure aqueous solutions include {100}, {111}, and {211}.

In the fractal regime individual crystallites are joined by successive epitaxial nucleations, exhibiting hexahedral (Figure 7) or octahedral (Figure 6) modifications, but not both simultaneously. The absence of the dodecahedron is due to the presence of the water molecules in the gel. In both fractal modifications the various crystallites are joined by the $2 \times 1$ icosahedral surface reconstruction by which a pair of pseudo-F-slices $d_{211}$ from the respective crystallites form a $2d_{211}$ epitaxial layer (Figure 4). For that reason the {211} form is not visible in any fractal patterns. The epitaxial reconstruction prevents the octahedron from appearing in the hexahedral habit. It also prevents the hexahedron from appearing in the octahedral habit.

In the theory of nucleation and growth kinetics,[1] the onset of the fractal morphology is marked by an increase in surface supersaturation and a structural match between parent and daughter crystallites. The increase in effective surface supersaturation is caused by the blocking action of the agarose molecules of the gel on the $NH_4Cl$ surfaces. The structural match is illustrated at the macroscopic level in Figure 1b of Ref 1. It is equivalent to the reconstructive epitaxial nucleation mechanism (SIREN) of Figure 4 introduced in this work.

The surface reconstruction on {211} is foreseen in all growth conditions. In fractal growth the crystallites are joined along {211} because reconstruction lends itself to nucleation. However, the onset of fractal growth depends crucially on increased surface supersaturation.[1] That increase is achieved in combination with the typically solution-triggered forms {100} and {111}. For that reason the epitaxial nucleation is characterized as solution-induced.

On the other hand, because {110} is a typically vapor habit, it arises in conditions of low surface supersaturations, and is therefore unlikely[1] to be accompanied by fractal growth and nucleation. In the hypothetical case that the fractal domain could be reproduced in an environment of low supersaturation, permitting the dodecahedron {110} to dominate, the present formulation speculates that epitaxial nucleation would persist by means of the {211} pyramidal faces, and become observable in a dodecahedral growth form.

The Hartman−Perdok theory applied at the molecular level leads to the same conclusions as the theory of nucleation and growth kinetics applied at the macroscopic level. Both formulations are in remarkable agreement with experimental results and

over a wide range of growth conditions, specifically fractal branching patterns emerging from agarose gel.

**Acknowledgment.** The authors are indebted to Dr. T. N. Kerestedjian of the Mineralogical Institute of the Bulgarian Academy of Sciences for providing information on sal-ammoniac and Figure 5. C.S.S. thanks The Netherlands Foundation for Research in Astronomy (ASTRON) for use of graphics facilities. M.W. thanks the NSF of China, the Chinese Committee of Science and Technology, and the Qiu Shi Foundation of Science and Technology.

## References and Notes

(1) Liu, X.-Y.; Strom, C. S. *J. Chem. Phys.* **2000**, *113*. In press.

(2) For example, see: Hartman, P. *Acta Crystallogr.* **1958**, *11*, 365, 459. Hartman, P. In *Crystal Growth: An Introduction*; Hartman, P., Ed.; North-Holland: Amsterdam, 1973; p 367. Hartman, P. The Dependence of Crystal Morphology on Crystal Structure. In *Growth of Crystals*; Sheftal, N. N., Ed.; Consultants Bureau: New York, 1969; Vol. 7, pp 3−18. Hartman, P.; Chan, H.-K. *Pharm. Res. 10* **1993**, 1052−1057.

(3) Strom, C. S.; et al. Ionic Crystals. In *Molecular Modeling Applications in Crystallization*; Myerson, A. S., Ed.; Cambridge University Press: New York, 1999; Chapter 5 and references therein.

(4) Strom, C. S. *Z. Kristallogr.* **1980**, *153*, 99; **1981**, *154*, 31; **1985**, *172*, 11.

(5) Strom, C. S.; Hartman, P. *Acta Crystallogr. A* **1989**, *45*, 371.

(6) Wang, M.; Liu, X.-Y.; Strom, C. S.; Bennema, P.; van Enckevort, W. J.; Ming, N.-B. *Phys. Rev. Lett.* **1998**, *80*, 3089−3092.

(7) Liu, X.-Y.; Wang, M.; Li, D.-W.; Strom, C. S.; Bennema, P.; Ming, N.-B. *J. Cryst. Growth* **2000**, *208*, 687−695.

(8) Groth, P. *Chemische Kristallographie*; Wilhelm Engelmann: Leipzig, 1906; pp 182−184.

(9) Strom, C. S. *J. Phys. Chem. B* **1999**, *103*, 11339−11345.

(10) Bartlett, G.; Langmuir, I. *J. Am. Chem. Soc.* **1921**, *43*, 84−91.

(11) Vainstein, B. K.; *Trudy Inst. Kristallogr. Akad. Nauk SSSR* **1956**, *12*, 18−24.

(12) Callanan, J. E.; Smith, N. O. *Adv. X-Ray Anal.* **1966**, *9*, 159−169.

(13) Sirdeshmukh, D. B.; Deshpande, V. T. *Acta Crystallogr. B* **1970**, *26*, 295.

(14) International Tables of X-ray Crystallography.

(15) Amethyst Galleries, Inc. 1997.

(16) Grimbergen, R.; Thesis, University of Nijmegen 1997.

(17) Hartman, P.; Heynen, W. M. M. *J. Cryst. Growth* **1983**, *63*, 261.

(18) Verheijen, M. A.; Vogels, L. J. P.; Meekes, H. *J. Cryst. Growth* **1996**, *60*, 337−345.